Journal of Power Sources 193 (2009) 349–358

Contents lists available at ScienceDirect

Journal of Power Sources

journal homepage: www.elsevier.com/locate/jpowsour

Electrolysis of carbon dioxide in Solid Oxide Electrolysis Cells

Sune Dalgaard Ebbesen*, Mogens Mogensen

Fuel Cells and Solid State Chemistry Division Risø National Laboratory for Sustainable Energy, Technical University of Denmark – DTU, Frederiksborgvej 399, 4000 Roskilde, Denmark

ARTICLE INFO

Article history:
Received 10 October 2008
Received in revised form 30 January 2009
Accepted 27 February 2009
Available online 19 March 2009

Keywords:
Solid Oxide Electrolysis Cell
SOEC
Carbon dioxide
Electrolysis
Synthetic fuel

ABSTRACT

Carbon dioxide electrolysis was studied in Ni/YSZ electrode supported Solid Oxide Electrolysis Cells (SOECs) consisting of a Ni-YSZ support, a Ni-YSZ electrode layer, a YSZ electrolyte, and a LSM-YSZ O_2 electrode (YSZ = Yttria Stabilized Zirconia). The results of this study show that long term CO_2 electrolysis is possible in SOECs with nickel electrodes.The passivation rate of the SOEC was between 0.22 and 0.44 mV h^{-1} when operated in mixtures of CO_2/CO = 70/30 or CO_2/CO = 98/02 (industrial grade) at 850 °C and current densities between −0.25 and −0.50 A cm^{-2}.

The passivation rate was independent of the current density and irreversible when operated at conditions that would oxidise carbon. This clearly shows that the passivation was not caused by coke formation. On the other hand, the passivation was partly reversible when introducing hydrogen. The passivation may be a consequence of impurities in the gas stream, most likely sulphur, adsorbing on some specific nickel sites in the cathode of the SOEC. Activation can be carried out by hydrogen reacting with adsorbed sulphur to form the volatile compound H_2S. Because adsorption of sulphur is site specific, only a part of the nickel sites were passivated and long-time operation of CO_2 electrolysis in these Ni/YSZ electrode supported Solid Oxide Electrolysis Cells seems therefore feasible.

1. Introduction

In recent years there has been an increased focus on hydrogen as an alternative energy carrier because of limited fossil fuel sources, increasing oil prices and environmental considerations. Water (steam) electrolysis ($H_2O \rightarrow H_2 + 1/2\ O_2$) in Solid Oxide Electrolysis Cells (SOEC) for production of hydrogen was under development as an interesting alternative to ordinary alkaline water electrolysis during the early 1980s [1,2]. The development of SOEC was slowed down around 1990 due to low fossil fuel prices, but has become increasingly investigated in the recent years as a green energy technology. Beside steam electrolysis, SOECs are also capable of electrolysing carbon dioxide to carbon monoxide and oxygen ($CO_2 \rightarrow CO + 1/2\ O_2$). Only limited studies have been reported for electrolysis of CO_2 in gas phase, where mainly palladium, platinum and nickel electrodes were used [2–13]. Recently CO_2 electrolysis was performed on ceramic cells with gadolinia-doped ceria cathodes [14]. NASA applied CO_2 electrolysis in SOECs as a mean for production of oxygen over both platinum and nickel cermets electrodes [2–7]. For production of oxygen, CO was treated as an undesired side product and converted back into CO_2 and carbon over an iron catalyst, and CO_2 was returned to the SOEC. Both *i–V* characterisation and long-time performance for 1600 h were reported on nickel based electrodes. Recently we showed *i–V* characterisation for CO_2 electrolysis in SOCs optimised for operation in fuel cell mode with significant lower resistance than previously reported for SOECs [9].

Co-electrolysis of steam and CO_2 in an SOEC yield synthesis gas ($CO + H_2$) which in turn can be catalysed to various types of synthetic fuels [15]. Using SOECs for recycling or reuse of CO_2 from energy systems (or CO_2 capture from air) would therefore be an attractive alternative to storage of CO_2 and would provide CO_2 neutral synthetic hydrocarbon fuels. The basic principle for a SOEC and SOFC operating on H_2O/H_2 and CO_2/CO is shown in Fig. 1.

From a thermodynamic point of view, it is advantageous to operate endothermic reactions, such as H_2O and/or CO_2 electrolysis, at high temperature because a larger part of the energy required for the reaction can then be obtained in the form of high temperature heat, e.g. heat form solar concentrators or waste heat from nuclear power plants [16–18]. Electrolysis in SOECs is typically performed in the temperature range from 750 to 1000 °C, and can therefore be operated with a lower electricity consumption compared to low temperature electrolysis [19,20]. Furthermore, reaction kinetics increases at high temperature which leads to a decreased internal resistance of the cell and thereby increased efficiency. Even though it is, from a thermodynamic and electrode kinetic point of view, advantageous to operate the SOECs at high temperature,

* Corresponding author. Tel.: +45 4677 5703.
E-mail addresses: Sune.Ebbesen@risoe.dk (S.D. Ebbesen), Mogens.Mogensen@risoe.dk (M. Mogensen).

0378-7753/$ – see front matter © 2009 Elsevier B.V. All rights reserved.
doi:10.1016/j.jpowsour.2009.02.093

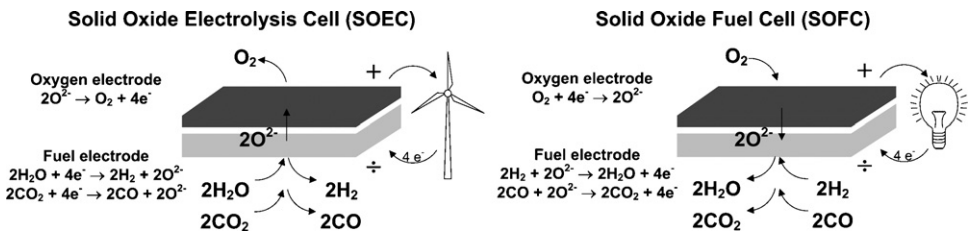

Fig. 1. Schematic presentation of the operational principle for a Solid Oxide Electrolysis Cell (SOEC) and a Solid Oxide Fuel Cell (SOFC).

material stability makes an upper limit for the operation temperature.

At high cell voltages reduction of carbon dioxide to coke, which can deposit on the active sites or within the porous electrode, may occur. Further, nickel is well known to catalyse dissociation of carbon containing gases or disproportionation of CO (Boudouard reaction) leading to the formation of, e.g. carbon nanofibers [21]. Carbon deposition on the active sites or within the porous electrode would reduce cell performance.

The regions for catalytic formation of coke in SOCs have been treated in great details and it was shown that formation of coke occur at very high CO concentrations only [22]. At realistic CO_2/CO concentrations during CO_2 electrolysis the equilibrium of the Boudouard reaction is shifted towards CO, and coke will therefore not be formed catalytically during electrolysis.

It is the aim of this study to examine the feasibility of CO_2 electrolysis in nickel based SOECs using the recently developed SOFC types of cells. Both initial performance and durability/degradation will be examined for CO_2/CO mixtures in Ni/YSZ electrode supported Solid Oxide Electrolysis Cells. The origin for the passivation will further be discussed.

2. Experimental

2.1. Solid oxide cell preparation

Planar Ni/YSZ supported cells of 5 cm × 5 cm with an active electrode area of 4 cm × 4 cm were used for the electrolysis tests. The cells were full cells produced at Risoe National Laboratory as previously described [23,24]. The cells have a 10–15 μm thick Ni/YSZ cermet electrode, a 10–15 μm thick YSZ electrolyte, a 15–20 μm thick strontium-doped lanthanum manganite (LSM) composite oxygen electrode. The cells are supported by a ∼300 μm thick porous Ni/YSZ layer [25]. The ratio between Ni and YSZ (TZ8Y, Tosoh Corporation, ZrO_2 stabilized with 8 mol% Y_2O_3) is 40/60 vol.% both for the support layer and the active electrode layer [26]. The composition of the LSM is $(La_{0.75}Sr_{0.25})_{0.95}MnO_3$ and the ratio between LSM and YSZ in the composite electrode is LSM/YSZ = 50/50 vol.% [27]. At start-up, nickel oxide in the Ni/YSZ electrode is reduced to nickel in hydrogen at 1000 °C.

2.2. Testing the solid oxide cells

For testing the cells, a test house as described in details elsewhere [28] and shown in Fig. 2 was used. The cell was sandwiched between the CO_2/CO and O_2/air gas distributor components, which were contacted with gold or nickel foils to pick up the electrode current. The gas distributor components were made of the same material as the respective electrodes. The cell was sealed at its edges between the two alumina blocks using glass bars. Gas channels for gas inlet and outlet were made in the alumina block. Current pick-up was achieved through the alumina block, which contain several voltage probes to indicate the voltage gradient along the electrodes (the so-called in-plane voltage). The in-plane voltages are usually below 1 mV due to the high conductivity of the metal foils. The in-plane voltage reflects that significant current flow inplane through the metal foil, e.g. due to uneven current density distribution over the cell. The test house was placed in a furnace to operate the cell at the desired temperature.

2.3. Characterisation of the solid oxide cells

For measurement of the nickel surface sites in the Ni/YSZ support layer, a Ni/YSZ support layer, identical to the support layer of the finish SOC, was produced. After reducing the nickel oxide to metallic nickel, the support layer was crushed to size and the nickel surface area was determined by CO chemisorption using 4 g of reduced Ni/YSZ in a volumetric system (Autosorb-1, Quantachrome). After 2 h of reduction at 400 °C, the sample was degassed and cooled to 40 °C. Subsequently, the CO adsorption isotherm was measured, and the CO chemisorption capacity (μmol $g^{-1}_{Ni/YSZ}$)

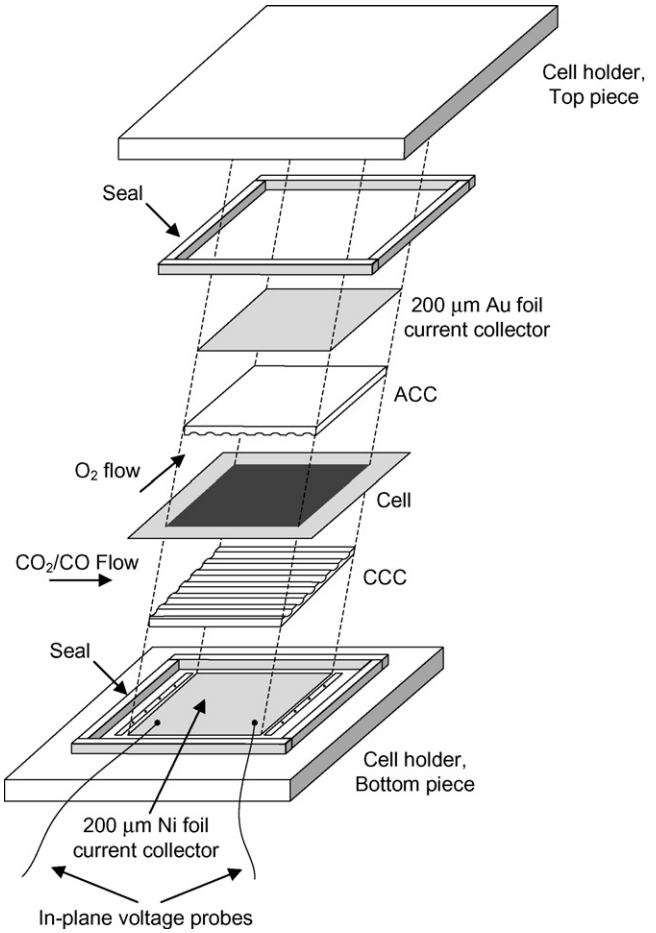

Fig. 2. The assembly of cell and gas distributor plates (ACC and CCC) in a cross-flow pattern, after [28].

Table 1
Operating conditions, measured cell voltage, ASR and passivation during the durability test for cell-1. The numbers correspond to the numbers in Fig. 4. The measured cell voltage corrosponds to Fig. 4 as well. ASRs are calculated from either the measured cell voltage and applied current, i.e. $ASR_{1,start}$ ($ASR = (V_{1,start(-0.25\,A\,cm^{-2})} - OCV/Current\ density(-0.25\,A\,cm^{-2}))$), or from the measured *i–V* curves, i.e. ASR_{i-V4a} (ASR_{i-V} = (Cell voltage at 0.25 A cm^{-2} − OCV/Current density (0.25 A cm^{-2}))).

Number		Time (h)	Gas composition to the Ni/YSZ electrode	Current density (A.cm^{-2})	Cell voltage (mV)	ASR (Ω cm^2)	Passivation (mV h^{-1})
1		0–150	CO_2/CO, 70/30	−0.25	$V_{1,\ start}$ = 1012 $V_{1,\ end}$ = 1050	$ASR_{1,\ start}$ = 0.37 $ASR_{1,\ end}$ = 0.52	0.2523
2		150–175	CO_2/CO, 70/30	0	V_2 = 918		
3		175–265	CO_2/CO, 70/30	−0.25	$V_{3,\ start}$ = 1051 $V_{3,\ end}$ = 1070	$ASR_{3,\ start}$ = 0.53 $ASR_{3,\ end}$ = 0.61	0.2165
4	4a		CO_2/CO, 70/30	i–V_{EL}		$ASR_{i-V\ 4a}$ = 0.61	
	4b	265–272	CO_2/CO, 70/30	i–V_{FC}		$ASR_{i-V\ 4b}$ = 0.55	
	4c		CO_2/CO, 70/30	i–V_{EL}		$ASR_{i-V\ 4c}$ = 0.61	
5		272–407	CO_2/CO, 70/30	−0.25	$V_{5,\ start}$ = 1172 $V_{5,\ end}$ = 1132	$ASR_{5,\ start}$ = 0.62 $ASR_{5,\ end}$ = 0.85	0.4368
6	6a	407–417	CO_2/CO, 70/30	0	V_{6a} = 918		
	6b	417–420	CO_2/CO, 70/30	−0.25	$V_{6b,\ start}$ = 1133 $V_{6b,\ end}$ = 1142	$ASR_{6b,\ start}$ = 0.86 $ASR_{6b,\ end}$ = 0.89	3.0606
	6c	420–429	CO_2/CO, 70/30	0	V_{6c} = 918		
	6d	429–432	CO_2/CO, 70/30	−0.25	$V_{6d,\ start}$ = 1143 $V_{6d,\ end}$ = 1152	$ASR_{6d,\ start}$ =0.90 $ASR_{6d,\ end}$ = 0.92	3.1457
	6e	432–439	CO_2/CO, 70/30	0	V_{6e} = 918		
	6f	439–442	CO_2/CO, 70/30	−0.25	$V_{6f,\ start}$ = 1155 $V_{6f,\ end}$ = 1166	$ASR_{6f,\ start}$ =0.95 $ASR_{6f,\ end}$ = 0.99	3.4317
	6g	442–447	CO_2/CO, 70/30	0	V_{6g} = 918		
	6h	447–450	CO_2/CO, 70/30	−0.25	$V_{6h,\ start}$ = 1160 $V_{6h,\ end}$ = 1171	$ASR_{6h,\ start}$ = 0.97 $ASR_{6h,\ end}$ = 1.01	1.8879
	6i	450–453	CO_2/CO, 70/30	0	V_{6i} = 918		
	6j	453–470	CO_2/CO, 70/30	−0.25	$V_{6j,\ start}$ = 1162 $V_{6j,\ end}$ = 1170	$ASR_{6j,\ start}$ = 0.97 $ASR_{6j,\ end}$ = 1.00	0.4011
	6k	470–483	CO_2/CO, 70/30	0	V_{6k} = 918		
	6l	483–497	CO_2/CO, 70/30	−0.25	$V_{6l,\ start}$ = 1173 $V_{6l,\ end}$ = 1186	$ASR_{6l,\ start}$ = 1.02 $ASR_{6l,\ end}$ = 1.07	0.9964
7	7a	497–502	CO_2/CO, 70/30	0	V_{7a} = 918		
	7b	502–507	H_2O/CO_2/CO, 4/67/29	0	V_{7b} = 912		
	7c	507–512	CO_2/CO, 70/30	0	V_{7c} = 918		
8		512–752	CO_2/CO, 70/30	−0.25	$V_{8,\ start}$ = 1187 $V_{8,\ end}$ =1197	$ASR_{1,\ start}$ = 1.07 $ASR_{1,\ end}$ = 1.11	0.0483
9		752–810	Gas-shift analysis	0			
10	10a	810–817	CO_2/CO, 70/30	0	V_{10a} = 918		
	10b	817	CO_2/CO, 70/30	i–V_{EL}		$ASR_{i-V\ 10b}$ = 1.13	
	10c	817–820	CO_2/CO, 70/30	0	V_{10c} = 918		
	10d	820–838	H_2/H_2O, 96/4	0	V_{10d} = 1.086		
	10e	838–840	CO_2/CO, 70/30	0	V_{10a} = 918		
11		840–1109	CO_2/CO, 70/30	−0.25	$V_{11,\ start}$ = 1151 $V_{11,\ end}$ = 1197	$ASR_{11,\ start}$ = 0.93 $ASR_{11,\ end}$ = 1.11	0.1703
		1109–1116	CO_2/CO, 70/30	0	$V_{CO_2/CO}$ = 918		
12	12a	1116	CO_2/CO, 70/30	i–V_{EL}		$ASR_{i-V\ 12a}$ = 1.09	
		(5h)	CO_2/CO, 70/30	0	$V_{CO_2/CO}$ = 918		
		(12h)	H_2	0	V_{H_2} = 1.141		
	12b	1143	CO_2/CO, 70/30	i–V_{EL}		$ASR_{i-V\ 12b}$ = 0.58	
		(21h)	H_2/CO_2/CO, 50/35/15	0	$V_{H_2/CO_2/CO}$ = 988		
	12c	1164	CO_2/CO, 70/30	i–V_{EL}		$ASR_{i-V\ 12c}$ = 0.46	
		(42h)	H_2/CO_2/CO, 50/35/15	0	$V_{H_2/CO_2/CO}$ = 988		
	12d	1206	CO_2/CO, 70/30	i–V_{EL}		$ASR_{i-V\ 12d}$ = 0.43	
		(65 h)	H_2/CO_2/CO, 50/35/15	0	$V_{H_2/CO_2/CO}$ = 988		
	12e	1271	CO_2/CO, 70/30	i–V_{EL}		$ASR_{i-V\ 12e}$ = 0.44	
		(1h)	CO_2/CO, 70/30	0	$V_{CO_2/CO}$ = 918		
		(1h)	H_2	0	V_{H_2} = 1.110		
	12f	1274	CO_2/CO, 70/30	i–V_{EL}		$ASR_{i-V\ 12f}$ = 0.44	
		(1h)	CO_2/CO, 70/30	0	$V_{CO_2/CO}$ = 918		
		(2h)	H_2	0	V_{H_2} = 1.110		
	12g	1277	CO_2/CO, 70/30	i–V_{EL}		$ASR_{i-V\ 12g}$ = 0.44	
		(1h)	CO_2/CO, 70/30	0	$V_{CO_2/CO}$ = 918		
		(4h)	H_2	0	V_{H_2} = 1.109		
	12h	1283	CO_2/CO, 70/30	i–V_{EL}		$ASR_{i-V\ 12h}$ = 0.43	

was calculated by extrapolation of the CO uptake to zero pressure [29].

2.3.1. Electrochemical characterisation of the solid oxide cells

After reduction, the cell was characterised in H_2O/H_2 mixtures following a standard procedure at Risø-DTU. This procedure includes DC and AC characterisation at varying atmosphere at both the Ni/YSZ electrode (4/96, 20/80 or 50/50 H_2O/H_2), and the LSM/YSZ electrode (pure oxygen or air, Technical air, Air Liquide). Steam was produced by reacting oxygen (industrial grade, $O_2 \geq 99.5\%$), Air Liquide) with hydrogen (N30, $H_2 \geq 99.9\%$, Air Liquide) at the inlet to the test housing.

DC characterisation of the cell was performed by recording polarization curves (i–V curves) in both electrolysis (except for 4% H_2O/H_2) and fuel cell mode by varying the current. The area-specific resistance (ASR) was calculated from the i–V curves as the chord from OCV to the cell voltage measured at a current density of $-0.25\,A\,cm^{-2}$ (electrolysis mode) or $0.25\,A\,cm^{-2}$ (fuel cell mode). When calculating the ASR from the i–V curves at current density of $-0.25\,A\,cm^{-2}$, the measured ASR for the i–V curves (denoted ASR_{i-V} = (Cell voltage at $-0.25\,A\,cm^{-2}$ − OCV)/(Current density ($-0.25\,A\,cm^{-2}$))) can be directly compared to the ASR measured during electrolysis at $-0.25\,A\,cm^{-2}$ (denoted ASR_x = (Cell voltage at time x($-0.25\,A\,cm^{-2}$) − OCV)/(Current density ($-0.25\,A\,cm^{-2}$)), where x refers to the time of measurement). The uncertainty for the ASRs calculated from the measured i–V curved is less than one percent.

AC characterisation at OCV was performed by electrochemical impedance spectroscopy using an external shunt and a Solartron 1255 or 1260 frequency analyzer.

After the standard characterisation in H_2O/H_2 mixtures, the hydrogen flow was slowly stepped to zero while first CO_2 (industrial grade, $CO_2 \geq 99.7\%$, Air Liquide) was added followed by the addition of CO (N20, CO ≥ 99.0%, Air Liquide). Additional DC and AC characterisation was performed in CO_2/CO mixtures with molar ratios of 50/50 or 70/30.

2.4. Durability of the Solid Oxide Electrolysis Cells

The durability of the Solid Oxide Cells during CO_2 electrolysis was examined for four identical cells. Electrolysis testing for cell-1 was performed in a CO_2/CO mixture with a molar ratio of 70/30. This cell was operated at a current density of $-0.25\,A\,cm^{-2}$, at OCV or i–V characterisation was performed. The only changes in the gas flow to the Ni/YSZ electrode were performed after 497 h, where the cell was set to OCV and steam was introduced, and after 800 or after 1100 h of operation, where hydrogen was introduced (Table 1). Further, a gas-shift analysis was performed after operation for 752 h. The gas-shift analysis consisted of AC characterisation identical to the initial AC characterisation. The operation conditions for the test are given in Table 1 together with the observed cell voltages.

Cell-2, cell-3 and cell-4 were operated at constant galvanostatic electrolysis conditions. Cell-2 and cell-3 were operated at $-0.25\,A\,cm^{-2}$ with a gas composition the Ni/YSZ electrode of CO_2/CO = 70/30 or CO_2/CO = 98/02 respectively. The cell voltage history and impedance for cell-2 was previously published in a proceedings paper [8]. Cell-4 was operated at $-0.5\,A\,cm^{-2}$ with a gas composition of CO_2/CO = 70/30.

In all cases, pure oxygen ($20\,L\,h^{-1}$) was passed over the oxygen electrode during electrolysis testing to avoid any transients in the polarization resistance, which depends on the oxygen partial pressure.

After successfully electrolysis operation for several hundreds of hours. All tests were stopped because of failures in the gas supply which damaged the cells. Consequently, no reliable post mortem analysis of the cells can be reported. Cell-1, cell-2, cell-3 and cell-4 were stopped after 1300, 370, 150 and 495 h of electrolysis testing respectively.

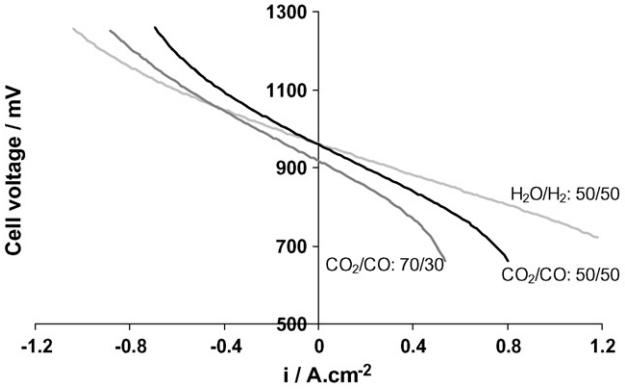

Fig. 3. Initial DC characterisation for cell-1 in CO_2/CO mixture (CO_2/CO = 50/50 and 70/30) and H_2O/H_2 mixture (H_2O/H_2 = 50/50) at 850 °C.

3. Results

3.1. Characterisation of the Solid Oxide Cells

The CO chemisorption capacity was measured to $3.32\,\mu mol\,g^{-1}{}_{Ni/YSZ}$. Assuming a stoichiometric factor of 1 for the adsorption of CO on nickel (CO/Ni = 1), the accessible nickel sites are $3.32\,\mu mol\,g^{-1}{}_{Ni/YSZ}$. The total weight of exposed Ni/YSZ support layer in this SOC/setup is approximately 2.5 g, resulting in a total of 8.30 μmol accessible nickel sites in the Ni/YSZ support layer of the SOC.

3.1.1. Initial electrochemical characterisation of the solid oxide cells

The initial performance of the cell was measured by recording i–V curves at 850 °C in both CO_2/CO and H_2O/H_2 mixtures. Fig. 3 shows a comparison of initial i–V curves measured in CO_2/CO mixtures (CO_2/CO = 50/50 and 70/30) with i–V curves measured in H_2O/H_2 mixtures (H_2O/H_2 = 50/50) for cell-1. Similar performance characteristics were measured for cell-2, cell-3 and cell-4.

From the i–V characteristic shown in Fig. 3, it is observed that no discontinuity occurs in the shift from fuel cell to electrolysis operation. The cell had an open-circuit voltage (OCV) of 962 and 959 mV at 850 °C for H_2O/H_2 = 50/50 and CO_2/CO = 50/50 respectively. The measured open-circuit voltage is in agreement with the Nernst potential (calculated from the Gibbs free energy of formation) for the mixtures ($E_{Nernst}^{50/50H_2O/H_2} = 963$ mV, $E_{Nernst}^{50/50CO_2/CO} = 959$ mV). Increasing the carbon dioxide concentration (CO_2/CO = 70/30) decreases the OCV to 918 mV, again in agreement with the Nernst potential ($E_{Nernst}^{70/30CO_2/CO} = 917$ mV). Similar OCVs were observed for cell-2, cell-3 and cell-4. In addition, increasing the carbon dioxide concentration for cell-4 (CO_2/CO = 98/02) decreases the OCV to 774 mV, again close to the Nernst potential ($E_{Nernst}^{98/02CO_2/CO} = 770$ mV).

The ASR in fuel cell mode was $0.22\,\Omega\,cm^2$ (calculated from the data in Fig. 3) for the cell when characterised in H_2O/H_2 = 50/50 at 850 °C in agreement with previous measurements for identical SOCs [30]. The ASR in electrolysis mode was $0.24\,\Omega\,cm^2$, showing a marginal higher activity towards oxidation of H_2 than reduction of H_2O for the Ni/YSZ electrode as reported previously [31,32]. The ASR for oxidation of CO, when operated in CO_2/CO mixtures with a ratio of 50/50 and 70/30 was 0.30 and $0.31\,\Omega\,cm^2$ respectively, showing lower activity for CO oxidation compared to H_2 oxidation in agreement with literature [33]. ASRs of 0.36 and $0.37\,\Omega\,cm^2$ were found for reduction of CO_2 in CO_2/CO mixtures with a ratio of 50/50

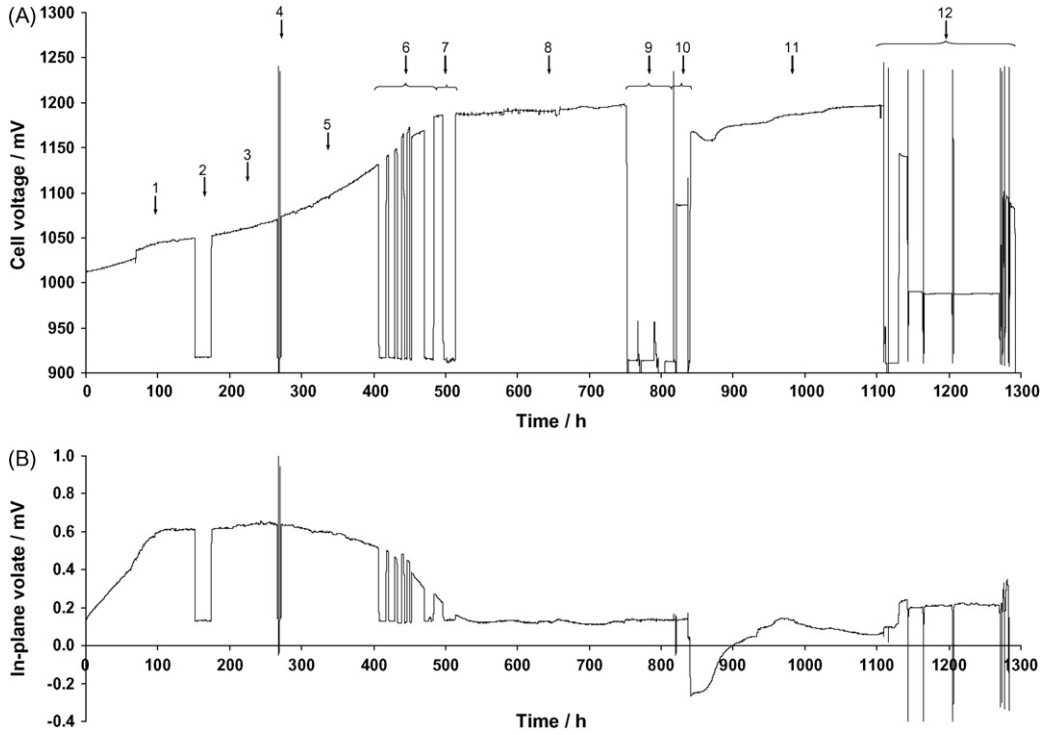

Fig. 4. (A) Cell voltage measured for cell-1 during electrolysis at −0.25 A cm^{-2} at 850 °C. (B) Corresponding in-plane voltage at the Ni/YSZ electrode. The gas composition to the negative Ni/YSZ electrode was a mixture of CO_2 and CO (CO_2/CO ratio of 70/30). See Table 1 for details. The five periods with constant electrolysis conditions are marked by the numbers 1, 3, 5, 8 and 11.

and 70/30 respectively. Thus a significant lower activity for CO_2 reduction than for CO oxidation was observed.

As predicted, lowering the temperature to 750 °C, showed an increased ASR (not shown). The ASR for oxidation of CO, when operated in CO_2/CO mixtures with a ratio of 50/50 and 70/30 was 0.50 and 0.52 Ω cm^2 respectively. ASRs of 0.53 and 0.58 Ω cm^2 were found for reduction of CO_2 in CO_2/CO mixtures with a ratio of 50/50 and 70/30 respectively. Again showing a significant lower activity for CO_2 reduction than for CO oxidation. Similar performance characteristics were measured for cell-2, cell-3 and cell-4.

3.1.2. Durability of the Solid Oxide Electrolysis Cells

3.1.2.1. Cell-1. After testing the initial performance of cell-1, durability in electrolysis mode was tested in a CO_2/CO mixture with a molar CO_2/CO ratio of 70/30. The operation conditions for the test are given in Table 1 together with the observed cell voltages, ASR values, and passivation rates.[1] The evolution of the cell voltage with time for the entire test is shown in Fig. 4. In Fig. 4, the five main electrolysis periods are marked by the numbers 1, 3, 5, 8 and 11. Between the first and second as well as between the third and fourth electrolysis period, the cell was kept at OCV. After operation for 497 h, steam was introduced into the cell at OCV (marked 7 in Fig. 4). Electrolysis period two and three (marked 3 and 5 in Fig. 4) was separated by recording *i–V* curves in both electrolysis and fuel cell mode; these *i–V* curves are shown in Fig. 5 and will be described in details later.

After operation for 820 h, hydrogen was introduced into the cell at OCV (marked 10 in Fig. 4). Finally a series of *i–V* curves was recorded in electrolysis mode only with introduction of pure H_2 or H_2/CO_2/CO in between (marked 11 and 12 in Fig. 4).

During the first electrolysis period, the cell voltage increased 38 mV over the first 150 h of electrolysis (corresponding to a passivation rate of 0.25 mV h^{-1}, Table 1). The increase in cell voltage after approximately 70 h of operation was caused by a brief cut off of oxygen to the oxygen electrode. During the second electrolysis period the passivation rate decreased slightly to 0.22 mV h^{-1}. Hereafter an increase in the passivation rate to 0.44 mV h^{-1} was observed for the third electrolysis period (period 5 in Fig. 4).

The cell voltage increased during the first three electrolysis periods, hereafter only little passivation was observed during the fourth electrolysis period (0.05 mV h^{-1}, Table 1). Introducing hydrogen into the cell at OCV (marked 10 in Fig. 4), significantly decreased the resistance for the cell ($ASR_{i-V\ 10b} > ASR_{11,start}$, Table 1). During the last electrolysis period (marked 11 in Fig. 4), the cell voltage

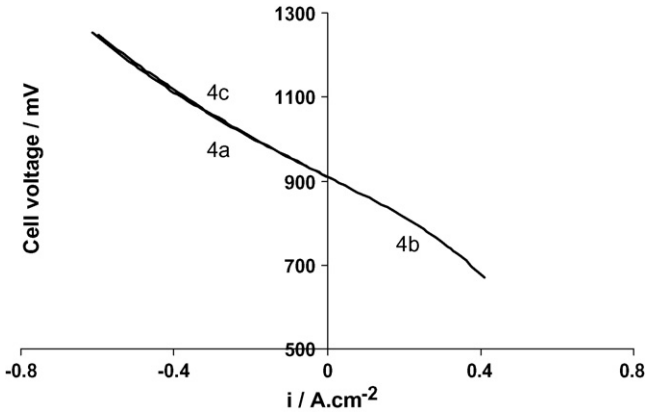

Fig. 5. *i–V* curves measured in both electrolysis and fuel cell mode after operating cell-1 for 265 h. The gas composition to the negative Ni/YSZ electrode was a mixture of CO_2 and CO (CO_2/CO ratio of 70/30). First one *i–V* curve was measure in electrolysis mode (marked 4a) followed by measuring of an *i–V* curve in fuel cell mode (marked 4b), finally a third *i–V* curve was measure in electrolysis mode (marked 4c).

[1] The term passivation is used to describe reversible loss in cell performance, whereas degradation describes an irreversible loss of performance. To describe a gain in performance, the term activation is used [34].

Table 2
Operating conditions, measured cell voltage, ASR and passivation during the durability tests of cell-2, cell-3 and cell-4. The measured cell voltages corresponds to Fig. 6.

Cell	Time (h)	Gas composition to the Ni/YSZ electrode	Current density (A cm^{-2})	Cell voltage (mV)	Passivation (mV h^{-1})
2	0–50	CO_2/CO, 70/30	−0.25	V_0 = 982 V_{50} = 1003	0.4370
	320–370	CO_2/CO, 70/30	−0.25	V_{320} = 1126 V_{370} = 1166	0.8909
3	0–50	CO_2/CO, 70/30	−0.50	V_{50} = 1084 V_{100} = 1106	0.4299
4	0–50	CO_2/CO, 98/02	−0.25	V_0 = 964 V_{50} = 971	0.1288
	200–250	CO_2/CO, 98/02	−0.25	V_{200} = 1011 V_{250} = 1045	0.6834
	340–390	CO_2/CO, 98/02	−0.25	V_{200} = 1153 V_{250} = 1284	2.6191
	440–490	CO_2/CO, 98/02	−0.25	V_{200} = 1290 V_{250} = 1295	0.0887

increased to exactly the same level as before introducing hydrogen ($V_{8,\mathrm{end}} = V_{11,\mathrm{end}}$, Table 1).

Electrolysis period one and two were separated by operating the cell at OCV. Furthermore the cell was set to OCV at varying duration with electrolysis operation at −0.25 A cm^{-2} in between as shown in Fig. 4 (marked 6). Although the cell was set to OCV, the passivation continued, which can be seen by the increase in cell voltage and ASR after the periods in OCV ($ASR_{3,\mathrm{start}} > ASR_{1,\mathrm{end}}$, and $ASR_{6b,\mathrm{start}} > ASR_{5,\mathrm{end}}$, etc. Table 1). The increase in cell voltage pr. hour was similar for period 6a, 6c and 6 g. The larger increase during period 6e, and the decrease during period 6i, was a consequence of a small instability in the gas supply resulting in small changes in the CO_2/CO ratio.

Electrolysis period two and three were separated by recording *i–V* curves in both electrolysis and fuel cell mode. First, one *i–V* curve was measured in electrolysis mode (marked 4a in Fig. 5 and Table 1) followed by measuring an *i–V* curve in fuel cell mode (marked 4b). Finally a third *i–V* curve was measured in electrolysis mode (marked 4c). The ASRs calculated from the *i–V* curves are 0.61, 0.55 and 0.61 Ω cm^2 for *i–V* curve 4a, 4b and 4c respectively (Table 1). Compared to the initial resistance ($ASR_{1,\mathrm{start}}$) of 0.37 Ω cm^2, the observed resistance were significantly increased.

After operation for 497 h, the cell was again set to OCV. At OCV steam was introduced (Fig. 4). Although the cell was set to OCV and steam was introduced, the passivation continued, which can be seen by the increase in cell resistance during electrolysis after introduction of steam ($V_{8,\mathrm{start}}$ = 1187 mV > $V_{6l,\mathrm{end}}$ = 1186 mV, Table 1).

After operation for 820 h, the cell was set to OCV, and an *i–V* curve was recorded (10b, Fig. 4). Subsequently hydrogen with four percent water (no CO_2 or CO) was introduced into the cell (10d, Fig. 4). Introduction of hydrogen caused a decrease in the ASR from 1.13 Ω cm^2 before introduction of hydrogen to 0.93 Ω cm^2 after introduction of hydrogen (Fig. 4).

Finally, after 1109 h of operation, a series of *i–V* curves was recorded in electrolysis mode only. The *i–V* curves were recorded in CO_2/CO = 70/30 with introduction of pure H_2 or H_2/CO_2/CO in between (marked 12 in Fig. 4 and Table 1). Again introduction of hydrogen activates the cell as the ASR reduces ($ASR_{i-V\,12a} > ASR_{i-V\,12b}$, Table 1). Also introducing mixture of H_2/CO_2/CO activates the cell ($ASR_{i-V\,12b} > ASR_{i-V\,12c} > ASR_{i-V\,12d}$). On the other hand, no further activation is observed when introducing pure hydrogen after operation for 1270 h ($ASR_{i-V\,12e} \sim ASR_{i-V\,12f} \sim ASR_{i-V\,12g} \sim ASR_{i-V\,12h}$).

The in-plane voltage for the Ni/YSZ electrode (Fig. 4B) increases initially corresponding to the increase in cell voltage. After operation for around 100 h the in-plane voltage levels off. Subsequently the in-plane voltage decrease to the same value as when the first electrolysis period was started. During the fourth electrolysis period (marked 8 in Fig. 4) where the cell voltage increased only little, the in-plane voltage remained close to stable. When introducing hydrogen after 820 h, a decrease to negative voltage occurs for the in-plane voltage. During the fifth electrolysis period, similar course as during the first 497 h of electrolysis was observed, i.e. an increase followed by a slight decrease in in-plane voltage.

3.1.2.2. Cell-2, Cell-3 and Cell-4. After testing the initial performance for cell-2, cell-3 and cell-4, durability in electrolysis mode was tested. The operation conditions for the three tests are given in Table 2 together with the observed cell voltages, and passivation rates. The evolution of the cell voltage with time for the three tests is shown in Fig. 6. As for cell-1, an increase in cell voltage was observed during electrolysis operation.

The increase in cell voltage for cell-2 and cell-3 (Fig. 6) was close to linear, similar to the initial period for cell-1 (Fig. 3) and cell-4 (Fig. 6). The initial passivation rate was similar for cell-2 and cell-3

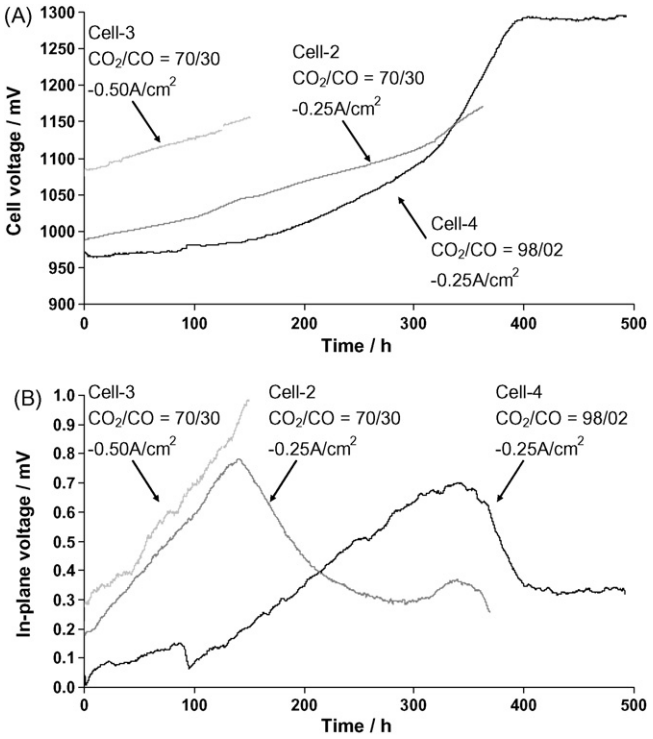

Fig. 6. (A) Cell voltage measured during electrolysis at 850 °C at either −0.25 A cm^{-2} (cell-2 and cell-4) or −0.50 A cm^{-2} (cell-3). (B) Corresponding in-plane voltage at the Ni/YSZ electrode. The gas composition to the negative Ni/YSZ electrode was a mixture of CO_2 and CO (for cell-2 and cell-3 the CO_2/CO ratio was 70/30 and for cell-4 the CO_2/CO ratio was 98/02).

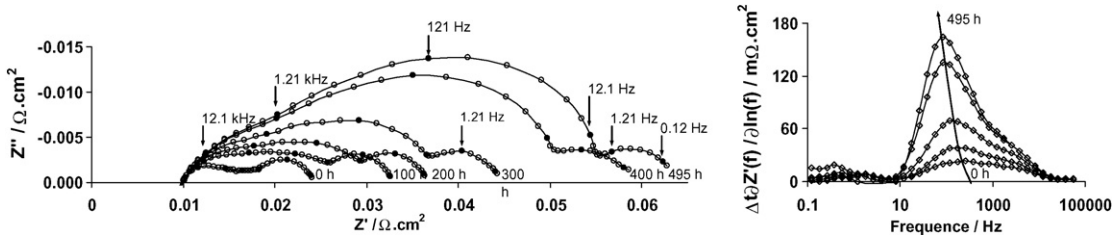

Fig. 7. (A) Nyquist plot of impedance spectra recorded during electrolysis for cell-1 and (B) ADIS during CO_2 electrolysis for cell-1, operated at $-0.25\,A\,cm^{-2}$ and 850 °C (CO_2/CO ratio of 70/30).

and was 0.44 and 0.43 mV h^{-1} respectively (Fig. 6, Table 2), this even that cell-3 was operated at higher current density ($-0.50\,A\,cm^{-2}$). The initial degradation rate for cell-4 was 0.13 mV h^{-1} only (Fig. 6, Table 2), which gradually increased to 2.62 mV h^{-1} after approximately 350 h of operation (Fig. 6, Table 2). As for cell-1, cell-4 passivated only partly, and the cell voltage reaches a plateau after 400 h with a limited passivation rate of 0.09 mV h^{-1} only (Fig. 6, Table 2). Cell-2 and cell-3 was not operated long enough to observe the plateau with low passivation.

The in-plane voltage for the Ni/YSZ electrode (Fig. 6B) increased initially for all three tests corresponding to the increase in cell voltage. Similar to cell-1, the in-plane voltages for cell-2 and cell-4 increases initially and goes through a maximum. Cell-3 was stopped before this maximum could be observed. After operating cell-4 for 400 h, the in-plane voltage remained close to stable during the following electrolysis period where the cell voltage increased only little.

3.1.2.3. AC characterisation during durability electrolysis testing. Electrochemical impedance spectra were recorded during the electrolysis tests to examine the cause of the passivation. Fig. 7A shows Nyquist plot of the impedance spectra recorded during the first three electrolysis periods for cell-1 (0–497 h of operation). To improve the frequency resolution of the spectra recorded during electrolysis testing, analysis of the difference in impedance spectra (ADIS) was performed [35]. The difference in the impedance spectra, were calculated from the real part of the experimental impedance, $Z'(f)$, according to equation (I) with $Z'(f)_{t=\text{start}}$ (start of electrolysis) used as the reference. The result of the ADIS ($\Delta_t \partial Z'(f)/\partial \ln(f)$) is shown in Fig. 7B.

$$\frac{\Delta_t \partial Z'(f)}{\partial \ln(f)} = \frac{(Z'(f)_{t=n+1} - Z'(f)_{t=\text{start}}) - (Z'(f)_{t=n-1} - Z'(f)_{t=\text{start}})}{\ln(f)_{n+1} - \ln(f)_{n-1}} \quad \text{(I)}$$

The initial impedance spectrum recorded during electrolysis consisted of two arcs with summits of 1.2 Hz and 2.6 kHz. The arc with a summit frequency of 1.2 Hz can be assigned to gas conversion and/or diffusion (0.1–10 Hz) [36]. The arc with a summit frequency of 2.6 kHz can be assigned to gas–solid (adsorption, dissociation, desorption) or solid–solid reaction (surface diffusion and oxygen transfer to/from the electrolyte) (1–50 kHz) [36]. After around 30 h of electrolysis a third arc started to develop at around 180 Hz, for which the summit frequency decreased to around 80 Hz during electrolysis. This arc may be assigned to diffusion (10 Hz–1 kHz) [37]. The ADIS over time during the electrolysis show that the main change occur around 80–180 Hz. Identical passivation characteristics (identical increase in impedance) was observed for cell-2 [8], cell-3 and cell-4.

From the impedance spectra, the ohmic resistance (R_s) can be found as the value of the real part of the impedance measured at 82 kHz. The polarization resistance (R_p) can be calculated as the difference in real part of the impedance at 0.38 Hz at 82 kHz. For all four tests, only a change in R_p occured, whereas R_s remain stable throughout the entire electrolysis test (0.14 Ω cm^2, cell-1, Fig. 7). The increase in R_p causes the increase in cell voltage. For cell-1, R_p increases from an initial value of 0.24 Ω cm^2 (corresponding to $ASR_{1,\text{start}}$ of 0.37 Ω cm^2) to 0.85 Ω cm^2 after 497 h of operation (corresponding to $ASR_{6l,\text{end}}$ of 1.07 Ω cm^2).

3.1.3. Gas-shift analysis for cell-1

Gas-shifts on both the Ni-YSZ and LSM electrodes were performed during the electrolysis test for cell-1 only (after 752 h of operation, Table 1). The gas-shifts allows for break down of the impedance contributions from each of the two electrodes. Prior to electrolysis, spectra were recorded at OCV first keeping the oxygen concentration to the oxygen electrode constant while recording spectra in CO_2/CO mixtures with a CO_2/CO ratio of 70/30 or 50/50. Afterwards the CO_2/CO composition to the Ni/YSZ electrode was kept constant, while spectra were recorded in pure oxygen and in synthetic air to the oxygen electrode (O_2/N_2 ratios of 21/79). A similar set of impedance spectra were recorded at OCV after electrolysis for 752 h. ADIS was performed by subtraction of two spectra where a gas-shift was made for one electrode only. The changes in impedance can be calculated according to Eq. (II), where $\partial Z'(f)_{\text{Ni/YSZ}}/\partial \ln(f)$ for the gas-shift at the Ni/YSZ electrode is shown (the difference for the LSM electrode can be calculated in similar manner):

$$\frac{\Delta_t \partial Z'(f)_{\text{Ni/YSZ}}}{\partial \ln(f)} = \frac{(Z'(f)_{\text{CO}_2/\text{CO}=50/50} - Z'(f)_{\text{CO}_2/\text{CO}=70/30})}{\partial \ln(f)} \quad \text{(II)}$$

The difference in impedance when changing the gas composition to the Ni/YSZ electrode from CO_2/CO = 70/30 to CO_2/CO = 50/50 while flowing pure oxygen to the oxygen electrode before and after electrolysis for 752 h is shown in Fig. 8A. The difference in impedance when changing the gas composition for the oxygen electrode from pure oxygen to synthetic air while CO_2/CO = 70/30 was flown to the Ni/YSZ electrode is shown in Fig. 8B. The difference in the gas-shift for either the Ni/YSZ or the LSM electrode is calculated as shown in equation (III), where $\Delta_{\text{gas-shift}}/\partial Z'(f)_{\text{Ni/YSZ}}/\partial \ln(f)$ for the gas-shift at the Ni/YSZ electrode is shown (the difference for the LSM electrode is calculated in similar manner). $\Delta_{\text{gas-shift}}/\partial Z'(f)_{\text{Ni/YSZ}}/\partial \ln(f)$ for the gas-shift analysis for cell-1 is shown in Fig. 8C.

$$\Delta_{\text{gas-shift}} \frac{\partial Z'(f)_{\text{Ni/YSZ}}}{\partial \ln(f)} = \frac{\partial Z'(f)_{\text{Ni/YSZ, after electrolysis}}}{\partial \ln(f)} - \frac{\partial Z'(f)_{\text{Ni/YSZ, before electrolysis}}}{\partial \ln(f)} \quad \text{(III)}$$

4. Discussion

The continuity of the *i–V* curves across OCV verifies that even though these solid oxide cells were developed and optimised for fuel cell use, they can work as reversible SOCs in both H_2O/H_2 and CO_2/CO mixtures.

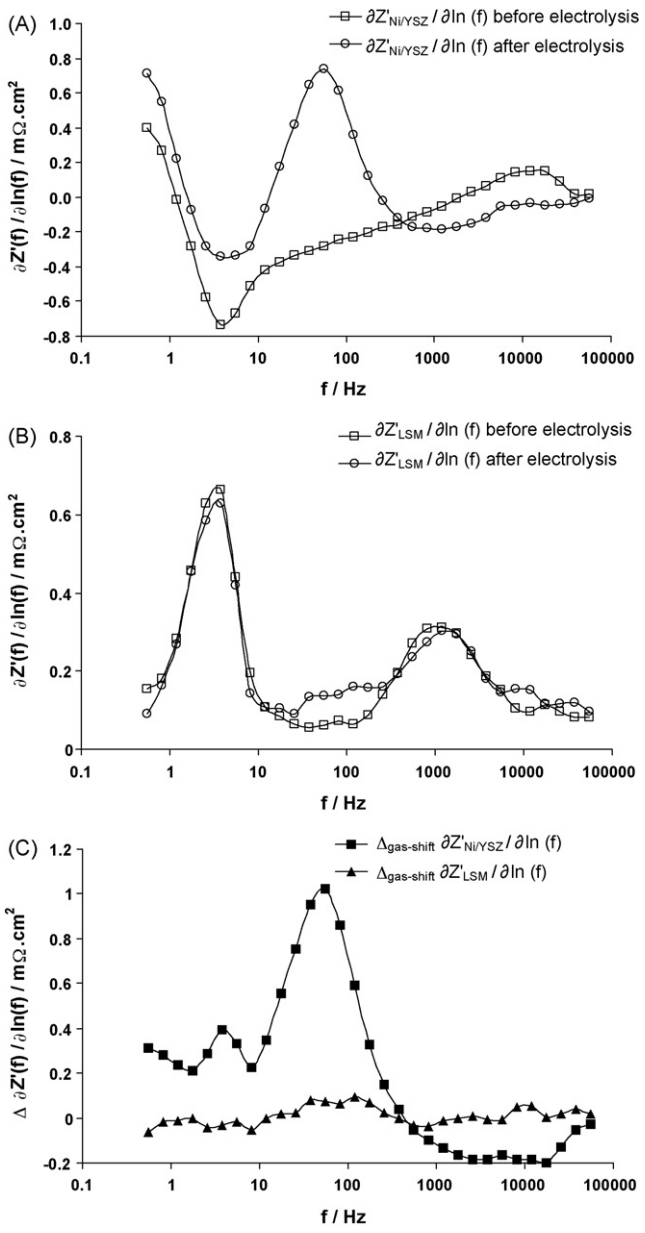

Fig. 8. Gas-shift analysis for cell-1. (A) Difference in impedance when changing the gas composition to the Ni/YSZ electrode (change in a CO_2/CO molar ratio from 70/30 to 50/50) while pure oxygen was flown to the oxygen electrode before and after electrolysis for 752 h. (B) Difference in impedance when changing the gas composition for the oxygen electrode from pure oxygen to synthetic air while CO_2/CO at a molar ratio of 70/30 was supplied to the Ni/YSZ electrode. (C) Difference in the gas-shift for either the Ni/YSZ or the LSM electrode.

A long-term passivation for the SOECs during CO_2 electrolysis was observed by the course of the cell voltage (Figs. 4 and 6) and the increase in impedance (Fig. 7). From the cell voltage shown in Fig. 4 and Fig. 6 it is evident that there is an long-term passivation rate between 0.22 and 0.44 mV h^{-1} during the first 400–500 h of electrolysis. The passivation rate for CO_2 electrolysis is thus comparable to the passivation rate of steam electrolysis at similar conditions for SOECs [20,31,34,38,39].

When performing ADIS on the gas-shift (Fig. 8), a significant change in $\partial Z'(f)$ is found for the Ni/YSZ electrode ($\partial Z'(f)_{Ni/YSZ}$) whereas only minor changes was observed for the oxygen electrode ($\partial Z'(f)_{LSM}$) (Fig. 8). This shows that the main passivation occurs at the Ni/YSZ electrode. The main difference observed for the Ni/YSZ electrode occurs at frequencies just around 80 Hz, which is consistent with the increase in impedance during electrolysis (Fig. 7).

When the cell was set to OCV any coke deposited within the porous Ni/YSZ electrode would be oxidised to CO according to the reverse Boudouard reaction (1) and thereby removed. Furthermore introducing steam is believed to remove coke depositions according to reaction (2).

$$C + CO_2 \rightarrow 2CO \quad (1)$$

$$C + H_2O \rightarrow CO + H_2 \quad (2)$$

That cell-1 cannot be activated by setting the cell to OCV and/or introduction of steam indicates that no coke had been formed, and the cell passivation is not a consequence of coke formation within the Ni/YSZ electrode. Any coke formed within the porous electrode would furthermore be removed by oxidation during measurement of the *i–V* curve in fuel cell mode after 265 h for cell-1 (Fig. 4, Fig. 5 and Table 1). Consequently, compared to the first *i–V* curve in electrolysis mode (marked 4a in Fig. 5 and Table 1), a lower ASR should be measured during the second *i–V* curve in electrolysis mode (marked 4c in Fig. 5 and Table 1). The identical ASRs for the *i–V* curves measured in electrolysis mode support that no coke was formed within the Ni/YSZ electrode. The differential impedance spectra recorded during electrolysis show that the main change occur around 80–180 Hz, which may be assigned to changes in gas diffusion [37] (Fig. 7). Increased diffusion limitations might be caused by the formation of coke in the porous Ni/YSZ electrode. During electrolysis the ohmic resistance (R_S) remained stable, whereas the polarization resistance (R_P) increased, which indicates that no structural changes occurred in the electrolyte/electrode interface region, e.g. break-up of the Ni particles or the cermet because of coke formation.

The in-plane voltage for the Ni/YSZ electrode shown in Figs. 4B and 6B, indicates that the cell passivation may be a transient phenomenon as has previously been reported for passivation/activation during steam electrolysis in SOECs [20] and during sulphur poisoning of SOFCs [40]. The deposition of impurities on specific sites would create a redistribution of the current as the resistance would be lower, where no impurities are deposited. Consequently a voltage gradient along the flow direction would occur. Because of the increasing passivated area, the in-plane voltage would increase until half of the cell is passivated. In this case, the passivated area is equal to the non-passivated area, and the maximal in-plane voltage would be observed. Likewise when more than the half of the cell is passivated, the in-plane voltage would start to decrease (corresponding to the smaller area with no passivation). Finally when the cell is fully passivated, no redistribution of the current takes place and the in-plane voltage would thus be identical to the initial in-plane voltage. The evolution of the in-plane voltage and that the degradation occurs on the Ni/YSZ electrode suggest that the SOEC passivate due to adsorption of impurities on active sites in the Ni/YSZ electrode as illustrated in Fig. 9. The course of the in-plane voltage during activation (introduction of hydrogen after 820 h of operation) indicates strongly, that only the area close to the inlet was activated, and this was passivated again during period 11.

For cell-1, the cell voltage at −0.25 A cm^{-2} was increased after periods of various duration at OCV (i.e. $V_{6b,end} > V_{6b,start}$). This indicates that the passivation is not a caused by the applied current density. The increase in cell voltage (and ASR) pr. hour is similar for period 6a, 6c and 6 g (Table 1). This is further supported when operating the cells at high current density (cell-3, 0.50 A cm^{-2}, CO_2/CO = 70/30) with identical passivation rate as when operated at low current density (cell-2, 0.25 A cm^{-2}, CO_2/CO = 70/30) (this passivation rate was however higher than the initial passivation rate for cell-1). This combined with the course of the in-plane shows that the cell passivation may be a consequence of impurities in the

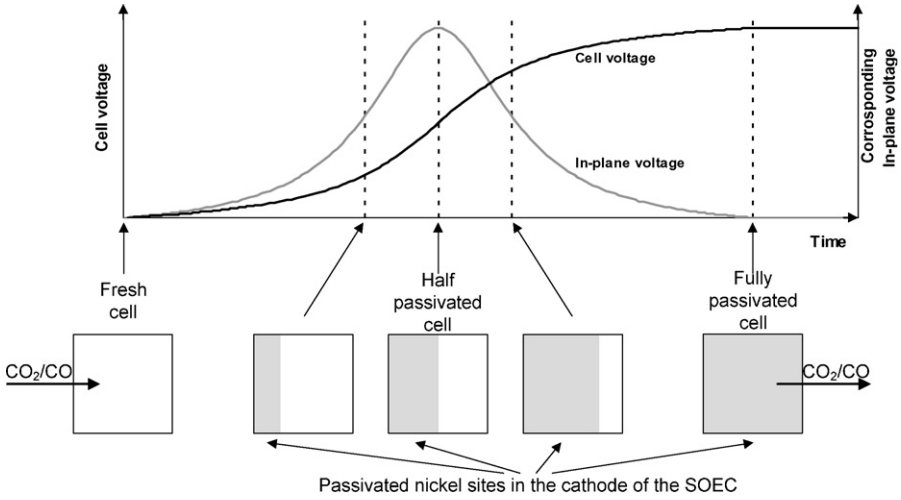

Fig. 9. Illustration of the evolution in in-plane and cell voltage due to passivation by adsorption of impurities (the impurities are illustrated by the gray area in bottom sketch) on nickel sites in the cathode of the SOEC.

gas stream, adsorbing on some specific active nickel sites in the cathode of the SOEC. Because the passivation is caused by impurities in the gas, reproducing the specific passivation rates is very difficult, i.e. the non-consistency in the passivation rate for the four tests.

Remarkably, cell-1 and cell-4 passivated only partly, i.e. the cell voltage reaches a plateau after 497 and 400 h, respectively, with only a limited passivation during the following electrolysis (cell-1: 0.05 mV h^{-1}, marked 8 in Fig. 4, and cell-4: 0.09 mV h^{-1}, Fig. 6). The faster passivation for cell-4 may indicate that CO_2 contain a higher impurity concentration than CO. For cell-1, the same cell voltage ($V_{11,\mathrm{end}}$ = 1197) was reached during the fifth electrolysis period after activation of the cell. This shows that only a part of the active sites are affected similar to sulphur poisoning of SOFCs [40,41]. That only a part of the active sites are affected shows that long-time operation of CO_2 electrolysis in these Ni/YSZ electrode supported SOECs is feasible.

4.1. Origin for passivation during CO_2 electrolysis

The course of the in-plane voltage strongly indicates, that the passivation is a consequence of impurities in the gas stream, adsorbing on specific active nickel sites in the cathode of the SOEC. Gas analysis by mass spectrometry (OmniStarTM GSD 301 01), of the CO_2 and CO revealed beside the expected mass fractions for CO_2 and CO (mass 44 (45, 46), 28 (29,30) and mass 16) also traces of argon (mass 40), oxygen (mass 32) and water (mass 18). Furthermore peaks at mass 33 and 34 were observed (intensity of mass 33 was approximately one third of the intensity of mass 34). The intensity of the peak at mass 34 was around 200 times to high to account for O^{18}. The peaks at mass 33 and 34 (and partly the peak at mass 32) may be assigned to traces of hydrogen sulphide (H_2S) as the base peak H_2S is located at mass 34, with secondary peaks at mass 33 (relative intensity of 43%) and mass 32 (relative intensity of 45%). Indeed the specifications from the provider of the gasses (Air Liquide) state that the gasses contain 5–8 ppb sulphur. This suggests that the passivation may be caused by sulphur impurities in the gas stream.

The poisoning effect of sulphur by chemisorption in Ni-based solid oxide fuel cells is well known. At low sulphur concentrations, the poisoning is believed to be caused by chemisorption of sulphur on the active nickel sites by the following reaction [42,43]:

$$H_2S_{(g)} \rightleftarrows S_{(ads)} + H_{2(g)(ads)} \quad (3)$$

Sulphur poisoning was shown to result in an initial passivation (voltage drop when operated in fuel cell mode) followed by a constant passivation [40,44–46]. The passivation was found to depend on H_2S concentration (deactivation levels off at increasing H_2S concentrations), current density when operated in fuel cell mode (deactivation is less at high current density) and temperature (deactivation is less at high temperature) [40,41,47–49]. It is generally accepted that the passivation caused by exposure to low amounts of H_2S is fully reversible (reaction (3)) [40,44,48,49]. When operated in fuel cell mode, adsorbed sulphur may oxidise to $SO_{2(g)}$ [44,48,47], explaining that sulphur only have a limited effect below approximately 55–60% of the saturation coverage [47]. Another explanation for the limited influence of small amounts of sulphur may be an initial replacement of strongly bound hydrogen with strongly bound sulphur [47]. Further, the adsorption of sulphur is site specific [50] which implies that sulphur only blocks a part of the active sites which may explain that the deactivation levels off at increasing H_2S concentrations.

The saturation coverage of sulphur on polycrystalline nickel ($Ni/MgAl_2O_4$) can be estimated to around 45% ($\theta_{\mathrm{Saturation}} = 0.45$) [51], in agreement with an observed increase in R_p of around 60% during hydrogen oxidation in an Ni/YSZ SOC [41] ($X_{R_p} = 1/1 - \theta \Rightarrow \theta = 0.40$). At a sulphur concentration of 5–8 ppb (specifications from Air Liquide), between 450 and 700 h are needed to introduce sufficient sulphur to the cell to obtain a S/Ni ratio of 0.45 in the support layer (8.3 μmol accessible nickel sites in the Ni/YSZ support layer, see above). Indeed the time needed to obtain saturation coverage of sulphur is in agreement with the 400–500 h of electrolysis operation needed to reach the plateau with low degradation (Figs. 4 and 6). This shows that the low sulphur concentration in the gas stream is sufficient to cause the observed passivation. It can further be speculated that the slow degradation at the plateau (0.05–0.09 mV h^{-1}) may be a consequence of the slow formation of nickel sulphide.

Activation of the cell is achieved when hydrogen reacts with adsorbed sulphur shifting the equilibrium of reaction (3) towards the volatile compound H_2S. The activation occurs at the inlet only. This show that the equilibrium is easily shifted away from H_2S towards adsorbed sulphur because of the strong adsorption of sulphur on nickel, similar to the slow reactivation behaviour of SOFCs after exposure to sulphur [40]. During introduction of $H_2/CO_2/CO$ the impurities are still introduced into the cell, nevertheless the introduction of hydrogen shifts the equilibrium of reaction 3 towards formation of the volatile compound H_2S.

It is our hypothesis that the passivation is a consequence of impurities, most likely sulphur, in the gas stream adsorbing on specific active nickel sites in the cathode of the SOEC. Initially sulphur adsorbs on the nickel sites in the support layer; when the majority of the nickel sites in the support layer at the inlet are covered by sulphur, sulphur may adsorb on the nickel sites in the electrochemically active layer. Consequently, an initial low passivation rate followed by an increase in passivation rate is observed. When saturation coverage of sulphur is obtained (because of site specific adsorption and equilibrium of reaction (6)), only minimal passivation is observed, resulting in the partly passivated cell (Figs. 4 and 6). Activation of the cell may be achieved by introducing hydrogen to form the volatile compound H_2S.

The slow passivation rate observed in the present study (passivated after 400–500 h only) combined with the impurity concentration in ppb levels show that SOECs are extremely sensible to impurities. Operation of SOCs in CO_2/CO mixtures may be more sensitive to sulphur then operation of SOCs in H_2O/H_2, because reaction (3) will be shifted towards adsorption (strong adsorption and no hydrogen), and when operated in electrolysis mode, where adsorbed sulphur cannot be removed by oxidation to SO_2 as suggested for SOFCs [44,48].

Presumable, the passivation can be avoided (or decreased) by cleaning the inlet gasses to the Ni/YSZ electrode. Attempts to perform clean experiments are undergoing. However, based on the low impurity concentration (ppb level) this is a very complicated task. Nevertheless, the cells only passivate partly, and long-time operation of CO_2 electrolysis in these Ni/YSZ electrode supported SOECs is feasible.

5. Conclusion

Electrolysis of CO_2 was performed in Solid Oxide Cells (SOCs) for several thousands hours at 850 °C. The cell passivation corresponds to 0.22–0.44 mV h^{-1} during the first 500 h of operation. After operation for 400–500 h the passivation reaches a plateau with moderate passivation only (0.05–0.09 mV h^{-1}). Long-time operation of CO_2 electrolysis in these Ni/YSZ electrode supported Solid Oxide Electrolysis Cells is therefore feasible. The passivation during CO_2 electrolysis is independent of the applied current density in the rage up to -0.50 A cm^{-2} and is irreversible when operated at conditions that oxidises carbon. The passivation is thus not caused by coke formation, but is caused by impurities, most likely sulphur, in the gas stream, adsorbing on specific nickel sites in the cathode of the Solid Oxide Electrolysis Cells. Reactivation of the cell can be achieved by introducing hydrogen, which reacts with adsorbed sulphur to form the volatile compound H_2S, which in turn is removed by the gas stream.

Acknowledgements

This work was financially supported by The Danish National Advanced Technology Foundations advanced technology platform "Development of 2nd generation bioethanol process and technology". The support from the staff of the Fuel Cells and Solid State Chemistry Department, Risø-DTU, is highly appreciated.

References

[1] W. Doenitz, R. Schmidberger, E. Steinheil, R. Streicher, Int. J. Hydrogen Energy 5 (1980) 55–63.
[2] A.O. Isenberg, Solid State Ionics 3–4 (1981) 431–437.
[3] L. Elikan, J.P. Morris, C.K. Wu, NASA Research Center, NASA Report CR-2014 (1972).
[4] A.O. Isenberg, C.E. Verostko, in: 19th Intersociety Conference on Environmental Systems, 1989) Paper 891506-.
[5] A.O. Isenberg, NASA Research Center, NASA Report CR-185612 (1989).
[6] A.O. Isenberg, R.J. Cusick, in: 18th Intersociety Conference on Environmental Systems, 1989) Paper 881040-.
[7] K.R. Sridhar, J. Br. Interplanet. Soc. 49 (1996) 435–440.
[8] S.D. Ebbesen, M. Mogensen, Proceedings of the 32nd International Conference & Exposition on Advanced Ceramics and Composites (ICACC), The American Ceramic Society, 2008, pp. 271–279.
[9] S.H. Jensen, P.H. Larsen, M. Mogensen, Int. J. Hydrogen Energy 32 (2007) 3253–3257.
[10] K.R. Sridhar, B.T. Vaniman, Solid State Ionics 93 (1997) 321–328.
[11] G. Tao, K.R. Sridhar, C.L. Chan, Solid State Ionics 175 (2004) 621–624.
[12] G. Tao, K.R. Sridhar, C.L. Chan, Solid State Ionics 175 (2004) 615–619.
[13] F. Bidrawn, G. Kim, G. Corre, J.T.S. Irvine, J.M. Vohs, R.J. Gorte, Electrochem, Solid State Lett. 11 (2008) B167–B170.
[14] R.D. Green, C.C. Liu, S.B. Adler, Solid State Ionics 179 (2008) 647–660.
[15] I. Chorkendorff, J.W. Niemantsverdriet, Concepts of Modern Catalysis and Kinetics, Wiley-VCH, Weinheim, 2006.
[16] B. Yidiz, M.S. Kazimi, Int. J. Hydrogen Energy 31 (2006) 77–92.
[17] J.E. O'Brien, C.M. Stoots, J.S. Herring, P.A. Lessing, J. Hartvigsen, S. Elangovan, Proceedings of ICONE12 12th International Conference on Nuclear Engineering, 2004.
[18] A. Hauch, S.H. Jensen, M. Menon, M. Mogensen, Proceedings of Risø International Energy Conference, Denmark, 2005, pp. 216–230.
[19] M. Mogensen, S.H. Jensen, A. Hauch, I. Chorkendorff, T. Jacobsen, Proceedings of the 7th European SOFC Forum, 2006.
[20] S.H. Jensen, Solid Oxide Electrolyser Cell, PhD Thesis, Risø National Laboratory, Roskilde, Denmark (2006).
[21] K.P. de Jong, J.W. Geus, Catal. Rev.-Sci. Eng. 42 (2000) 481–510.
[22] K. Sasaki, Y. Taraoka, J. Electrochem. Soc. 150 (2003) A885–A888.
[23] A. Hagen, R. Barfod, P.V. Hendriksen, Y.L. Liu, S. Ramousse, J. Electrochem. Soc. 153 (2006) A1165–A1171.
[24] P.H. Larsen, C. Bagger, S. Linderoth, M. Mogensen, S. Primdahl, M.J. Jorgensen, P.V. Hendriksen, B. Kindl, N. Bonanos, F.W. Poulsen, K.A. Maegaard, Proceedings - Electrochemical Society, 2001, pp. 28–37.
[25] P.H. Larsen, C. Bagger, S. Linderoth, M. Mogensen, S. Primdahl, M.J. Jørgensen, P.V. Hendriksen, B. Kindl, N. Bonanos, F.W. Poulsen, K.A. Maegaard, Proceedings of Solid Oxide Fuel Cell VII (SOFC VII), Electrochem. Soc., 2001, pp. 28–37.
[26] C. Bagger, Fuel Cell Seminar, Courtesy Associations, Inc., Washington, DC, 1992, p. 241.
[27] M.J. Jørgensen, M. Mogensen, J. Electrochem. Soc. 148 (2001) A433–A442.
[28] M. Mogensen, P.V. Hendriksen, High temperature solid oxide fuel cells—fundamentals design and applications, Elsevier, London, 2003, p. 261.
[29] J.E. Benson, H.S. Hwang, M. Boudart, J. Catal. 4 (1965) 704–710.
[30] N. Christiansen, J.B. Hansen, H. Holm-Larsen, S. Linderoth, P.H. Larsen, P.V. Hendriksen, A. Hagen, Proceedings of Risø International Energy Conference, Denmark, 2007.
[31] A. Hauch, S.H. Jensen, S. Ramousse, M. Mogensen, J. Electrochem. Soc. 153 (2006) A1741–A1747.
[32] O.A. Marina, L.R. Pederson, M.C. Williams, G.W. Coffey, K.D. Meinhardt, C.D. Nguyen, E.C. Thomsen, J. Electrochem. Soc. 154 (2007) B452–B459.
[33] P. Holtappels, L.G.J. de Haart, U. Stimming, I.C. Vinke, M. Mogensen, J. Appl. Electrochem. 29 (1999) 561–568.
[34] A. Hauch, S.H. Jensen, J.B. Bilde-Sørensen, M. Mogensen, J. Electrochem. Soc. 154 (2007) A619–A626.
[35] S.H. Jensen, A. Hauch, P.V. Hendriksen, M. Mogensen, N. Bonanos, T. Jacobsen, J. Electrochem. Soc. 154 (2007) B1325–B1330.
[36] S. Primdahl, M. Mogensen, J. Electrochem. Soc. 145 (1998) 2431–2438.
[37] S. Primdahl, M. Mogensen, J. Electrochem. Soc. 146 (1999) 2827–2833.
[38] A. Hauch, Solid Oxide Electrolysis Cells—Performance and Durability, PhD Thesis, Risø National Laboratory, Roskilde, Denmark (2007).
[39] A. Hauch, S.D. Ebbesen, S.H. Jensen, M. Mogensen, J. Electrochem. Soc. 155 (2008) B1184–B1193.
[40] J.F.B. Rasmussen, A. Hagen, J. Power Sources 191 (2009) 534–541.
[41] S. Primdahl, M. Mogensen, Solid Oxide Fuel Cells (Sofc Vi) 99 (1999) 530–539.
[42] M.Y. Gong, X.B. Liu, J. Trembly, C. Johnson, J. Power Sources 168 (2007) 289–298.
[43] Z. Cheng, M.L. Liu, Solid State Ionics 178 (2007) 925–935.
[44] S.W. Zha, Z. Cheng, M.L. Liu, J. Electrochem. Soc. 154 (2007) B201–B206.
[45] K. Sasaki, K. Susuki, A. Iyoshi, M. Uchimura, N. Imamura, H. Kusaba, Y. Teraoka, H. Fuchino, K. Tsujimoto, Y. Uchida, N. Jingo, J. Electrochem. Soc. 153 (2006) A2023–A2029.
[46] J.P. Trembly, A.I. Marquez, T.R. Ohrn, D.J. Bayless, J. Power Sources 158 (2006) 263–273.
[47] J.B. Hansen, Electrochem. Solid State Lett. 11 (2008) B178–B180.
[48] Z. Cheng, S. Zha, M. Lui, J. Power Sources 172 (2007) 688–693.
[49] Y. Matsuzaki, I. Yasuda, Solid State Ionics 132 (2000) 261–269.
[50] C.H. Bartholomew, Appl. Catal. A 212 (2001) 17–60.
[51] I. Alstrup, J.R. Rostrup-Nielsen, S. Røen, Appl. Catal. 1 (1981) 303–314.